





Rapid chemically selective 3D imaging in the mid-infrared: supplement

ERIC O. POTMA,^{1,2,6,†}  DAVID KNEZ,¹ YONG CHEN,³ YULIA DAVYDOVA,¹ AMANDA DURKIN,² ALEXANDER FAST,²  MIHAELA BALU,² BRENNAN NORTON-BAKER,¹ RACHEL W. MARTIN,^{1,4} TOMMASO BALDACCHINI,^{1,5}  AND DMITRY A. FISHMAN^{1,†,*} 

¹Department of Chemistry, University of California Irvine, California 92697, USA

²Beckman Laser Institute, University of California Irvine, California 92697, USA

³Epstein Department of Industrial and Systems Engineering, University of Southern California, Los Angeles, California 90089, USA

⁴Department of Molecular Biology & Biochemistry, University of California Irvine, California 92697, USA

⁵Current address: Edwards Life Sciences, Irvine, California 92612, USA

⁶e-mail: epotma@uci.edu

*Corresponding author: dmitryf@uci.edu

[†]These authors contributed equally to this paper.

This supplement published with The Optical Society on 7 July 2021 by The Authors under the terms of the [Creative Commons Attribution 4.0 License](https://creativecommons.org/licenses/by/4.0/) in the format provided by the authors and unedited. Further distribution of this work must maintain attribution to the author(s) and the published article's title, journal citation, and DOI.

Supplement DOI: <https://doi.org/10.6084/m9.figshare.14794077>

Parent Article DOI: <https://doi.org/10.1364/OPTICA.426199>

Supplementary Information

Rapid chemically selective 3D imaging in the mid-infrared

Eric O. Potma^{1,2,*,**}, David Knez¹, Yong Chen³, Yulia Davydova¹, Amanda Durkin², Alexander Fast², Mihaela Balu², Brenna Norton-Baker¹, Rachel W. Martin¹, Tommaso Baldacchini^{1,#}, Dmitry A. Fishman^{1,*,**}

¹ *Department of Chemistry, University of California Irvine, 92697 CA, United States*

² *Beckman Laser Institute, University of California Irvine, 92697 CA, United States*

³ *Epstein Department of Industrial and Systems Engineering, Los Angeles, CA 90089, United States*

⁴ *Department of Molecular Biology & Biochemistry, University of California Irvine, 92697 CA, United States*

currently with Edwards Life Sciences, Irvine, 92612 CA, United States

* these authors contributed equally

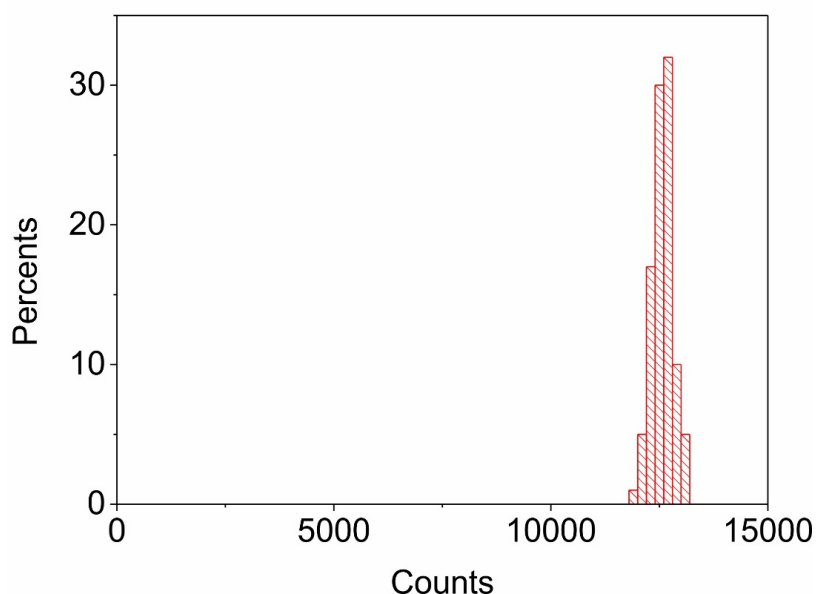
** dmitryf@uci.edu

epotma@uci.edu

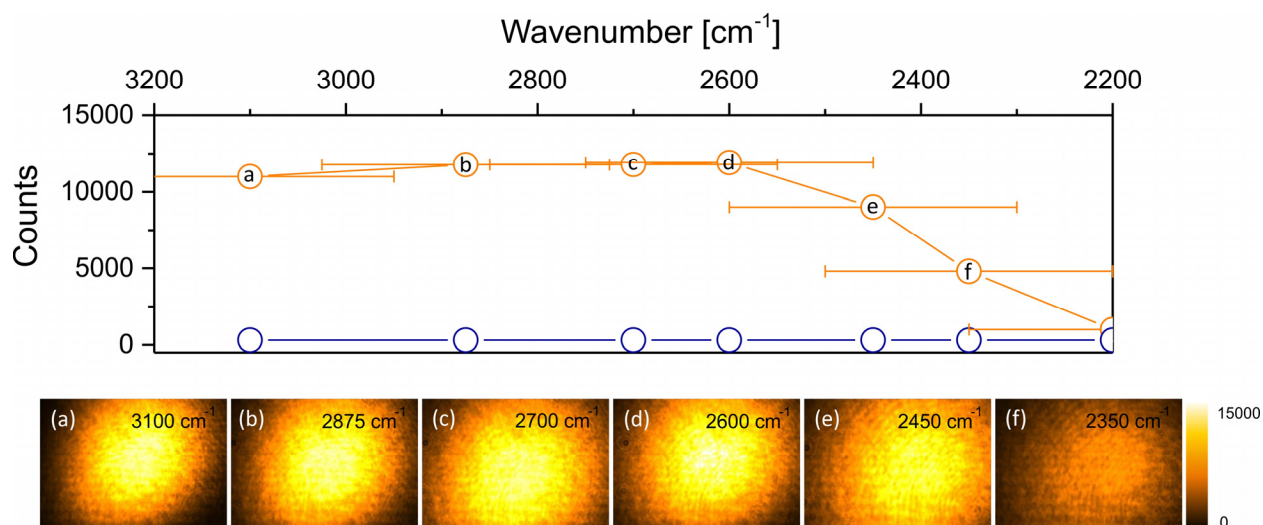
Supplementary Table 1. Experimental parameters.

MIR pulse width	~110 fs
MIR power	1.5 mW @ 1 kHz (not accounted for camera window absorption)
NIR power	0.15 mW @ 1 kHz
MIR spot size	3.5 mm
NIR spot size	4 mm
Pixel size	6.5 mm x 6.5 mm
CCD active area	1392x1040 pixels
Signal-to-noise ratio	
$10 \cdot \lg\left(\frac{S_{NTA}}{\sigma_{DTA}}\right)$	34 dB
Signal-to-noise ratio (mean power root)	
$20 \cdot \lg\left(\frac{S_{NTA}}{\sigma_{DTA}}\right)$	68 dB
Signal-to-background	
Signal-to-noise ratio	
$10 \cdot \lg\left(\frac{S_{NTA}}{S_{DTA}}\right)$	15 dB
Estimated quantum efficiency for MIR only*	$1 \cdot 10^{-9}$

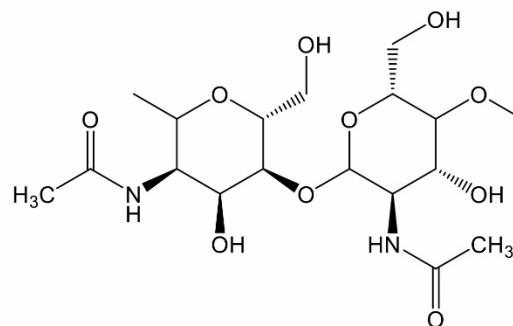
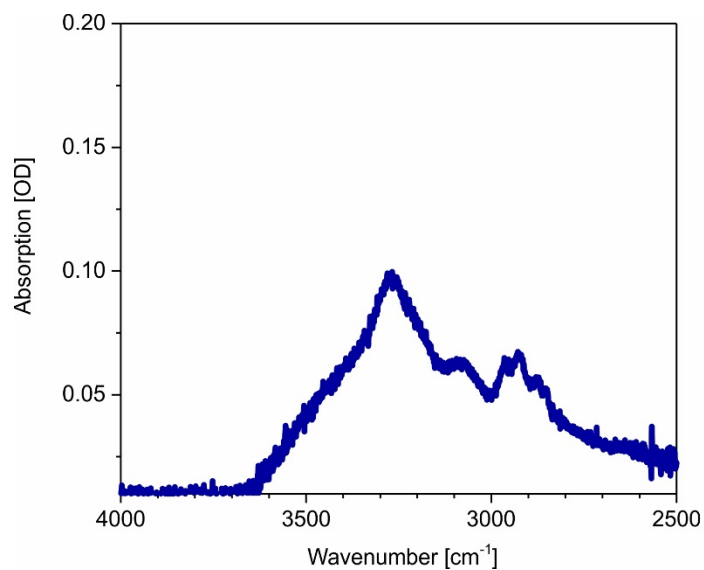
* Note that the standard definition of quantum efficiency is not applicable because NTA detection relies on both the number of NIR and MIR photons



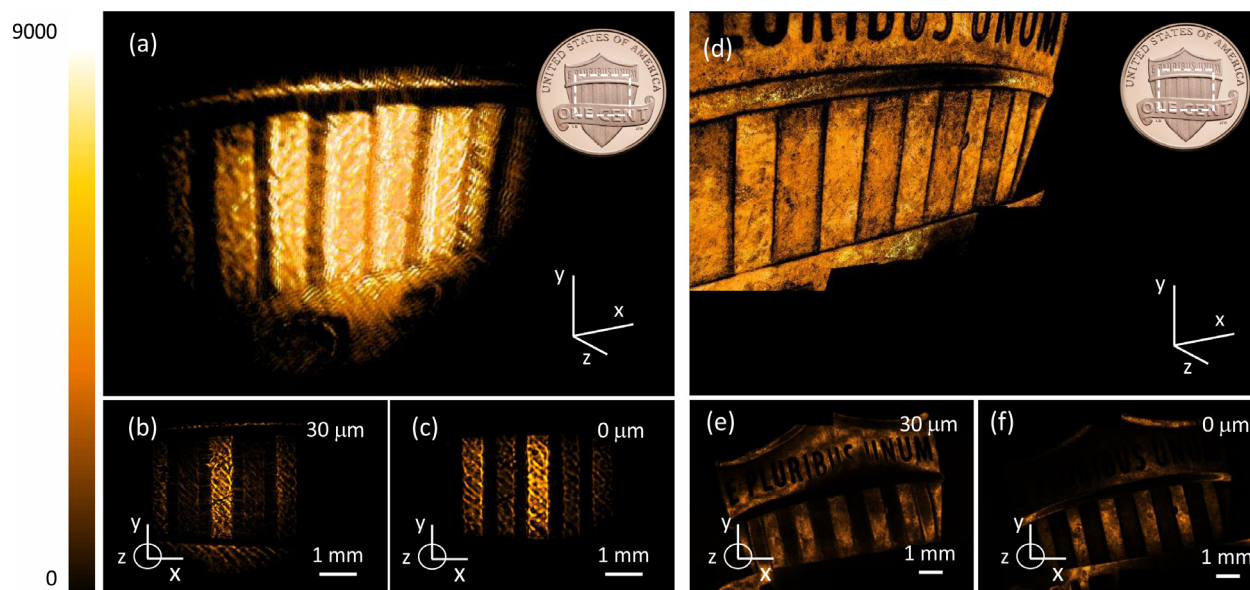
Supplementary Figure S1. Beam intensity stability for a single pixel at the center of the beam at 2850 cm^{-1} .
¹ Standard deviation $\sigma=0.019$ measured for 100 s integration time with 0.1 s frame rate.



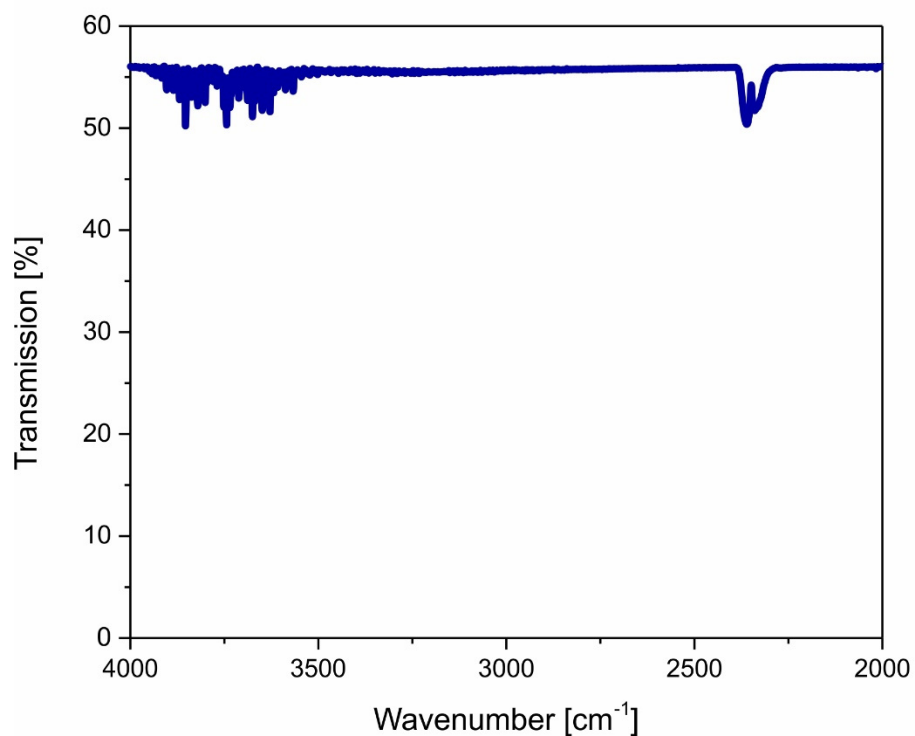
Supplementary Figure S2. Spectral response of detection system to MIR pulse reflected off a gold mirror (orange dots represent average counts within the center of gaussian beam, blue dots represent constant DTA background of the NIR beam). Average power flux is 4 mW/cm^2 prior to the camera and the exposure time is 100 ms for all measurements. Horizontal lines represent estimated Fourier limited spectral bandwidth of the 110 fs MIR pulse.



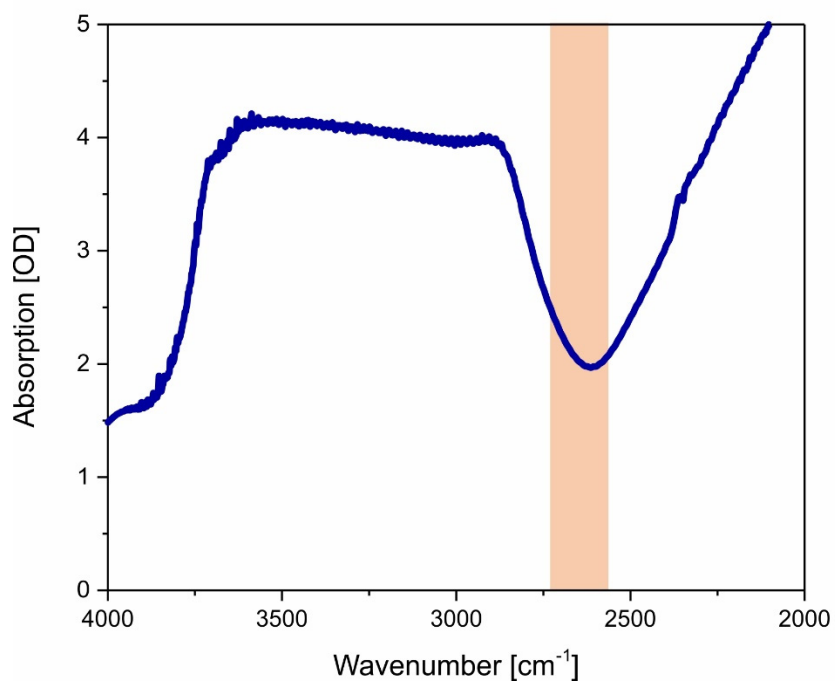
Supplementary Figure S2. FTIR-ATR spectrum of chitin (bee wing).



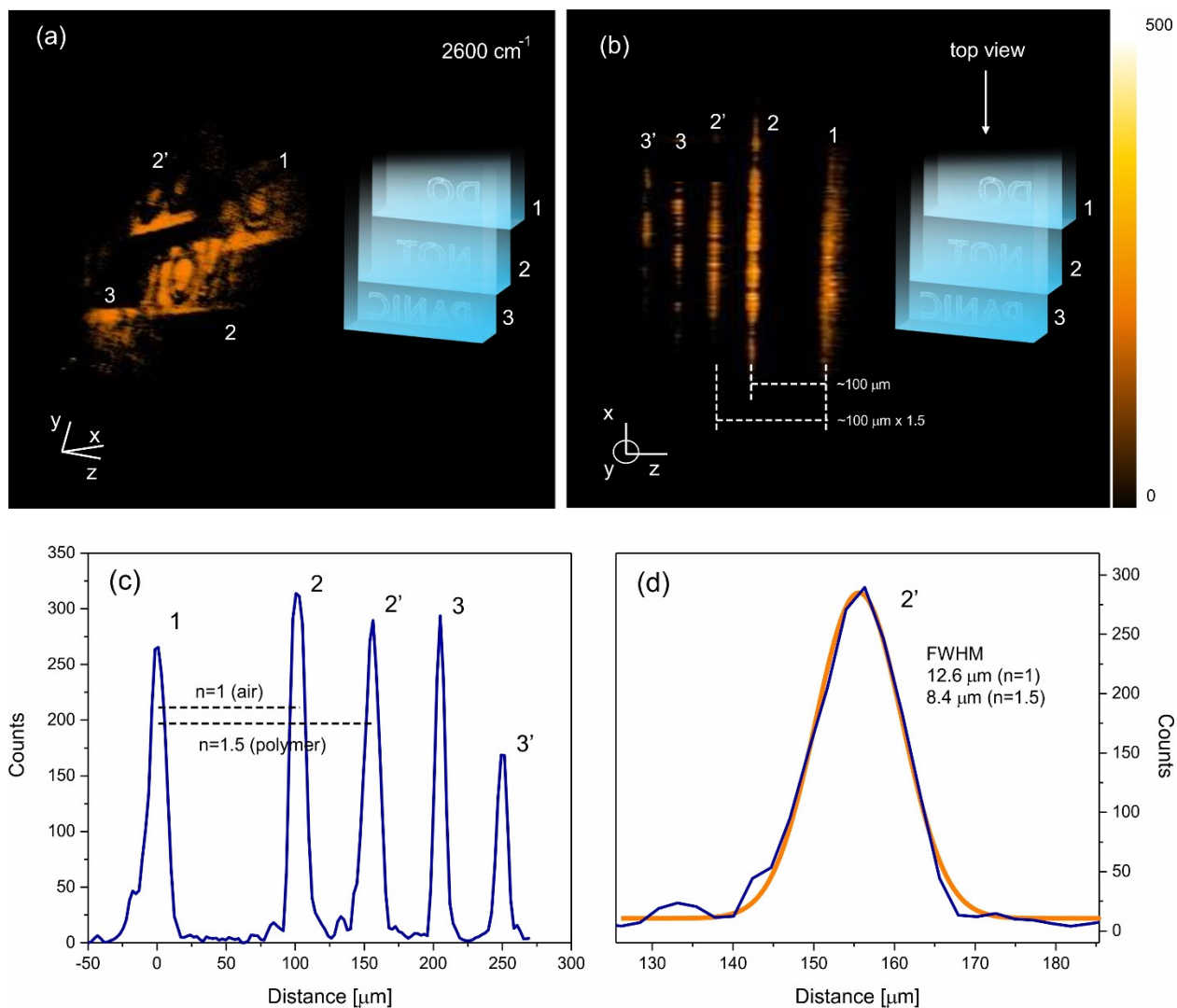
Supplementary Figure S3. (a, b, c) Tomographic imaging of the structured metal surface of a one cent US coin (Union Shield). (a) 3D reconstruction, (b) and (c) are frames measured at height $h=30\ \mu\text{m}$ and $h=0\ \mu\text{m}$, respectively. (d) 3D reconstruction of confocal reflection imaging of the coin. (e) and (f) are 2D confocal scans measured at height difference $30\ \mu\text{m}$.



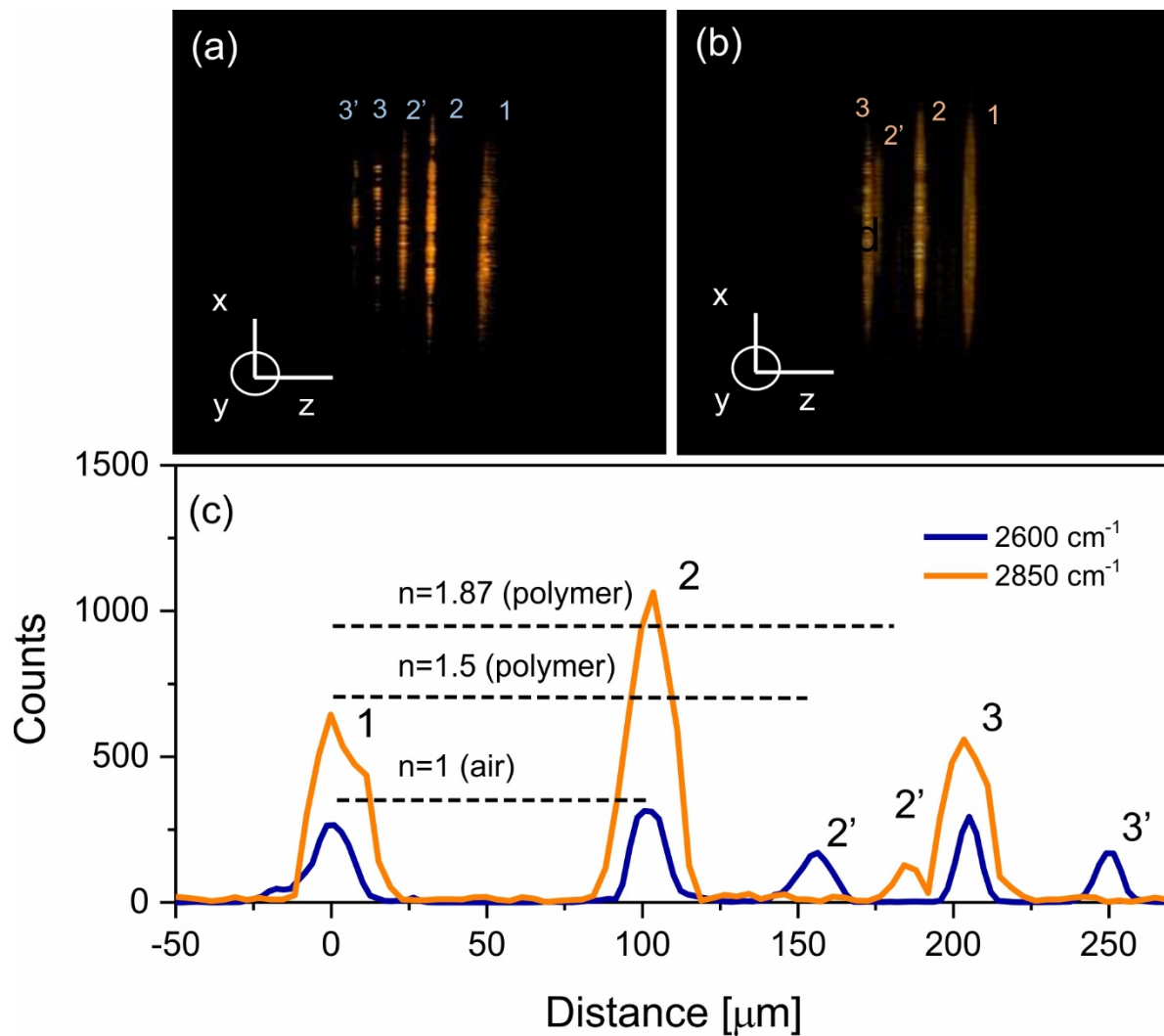
Supplementary Figure S4. FTIR transmission spectrum of a 3 mm GaAs wafer. Main IR light loss attributed to Fresnel reflection at the semiconductor/air interfaces. In double path, this results in ~25% transmission.



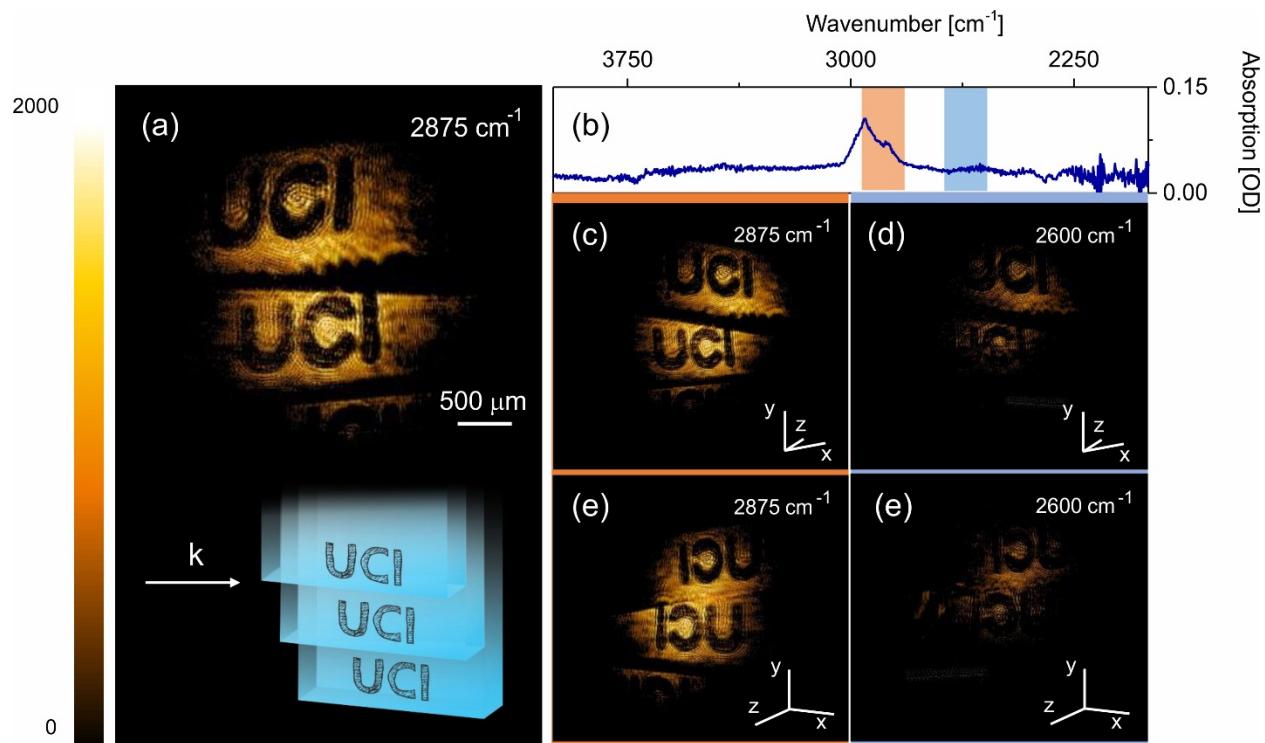
Supplementary Figure S5. FTIR transmission spectrum of a 380 μm water layer. Rectangle represents pulse spectral bandwidth.



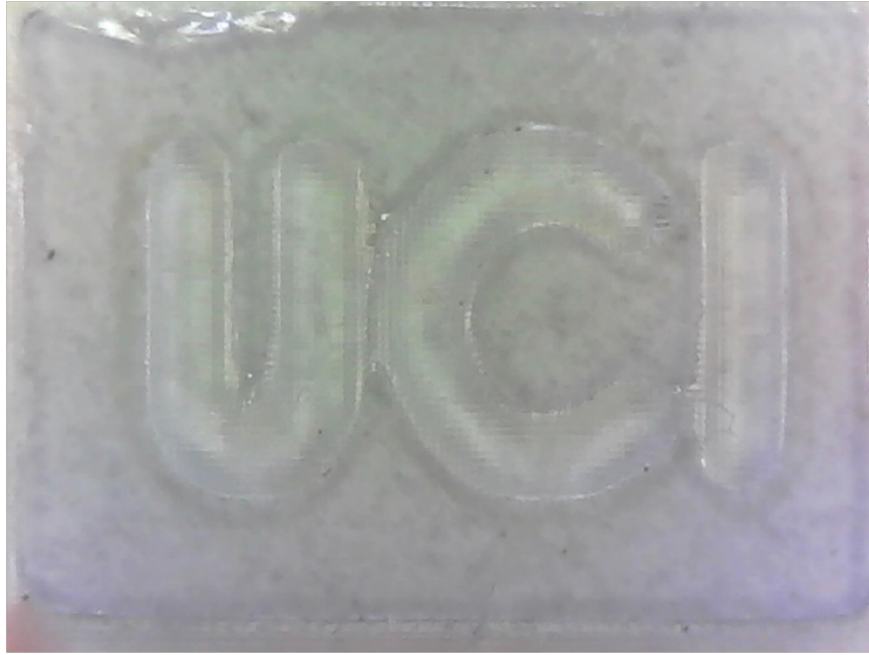
Supplementary Figure S6. 3D imaging of cellulose acetate transparency ladder at 2600 cm^{-1} shown at different perspective angles (a) and (b). Though reflected from the same surface 2, photons propagating through cellulose acetate sheet 1 are temporally delayed (2') with respect to photons that travel in air (2). (c) Spatial cross-section of MIR pulse propagation in layered cellulose acetate structure. (d) Gauss fit for response on 2' interface (propagation through cellulose acetate). FWHM indicates spatial resolution of $12.6\text{ }\mu\text{m}$.



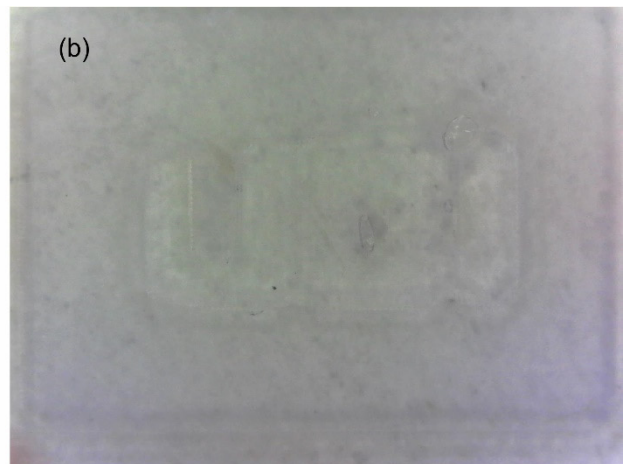
Supplementary Figure S7. 3D image of cellulose acetate structure imaged at 2600 cm⁻¹ and 2850 cm⁻¹ for top view perspective similar to Figure SF5b. (c) Peak positions of reflections off the different interfaces. The difference between the peak positions found for propagation in air and polymer reveals that $n \sim 1.5$ for 2600 cm⁻¹ and $n \sim 1.87$ for 2850 cm⁻¹.



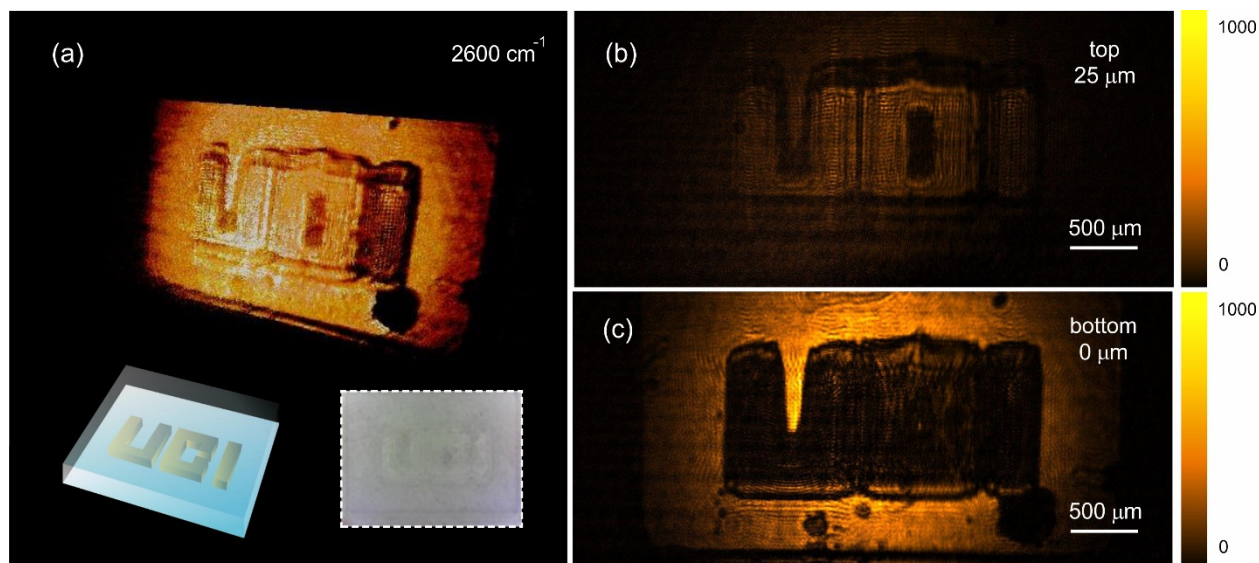
Supplementary Figure S8. 3D imaging of cellulose acetate transparency ladder. (a) 3D reconstruction of transparency ladder with printed letters. (b) FTIR transmission spectrum of cellulose acetate sheet. Rectangles represent Gaussian pulse width of ~ 150 cm⁻¹. (c) and (e) 3D imaging at 2850 cm⁻¹, (d) and (f) 3D imaging at 2600 cm⁻¹. Total 3D image acquisition time is 1s.



Supplementary Figure S9. Optical image of designed resin structure.

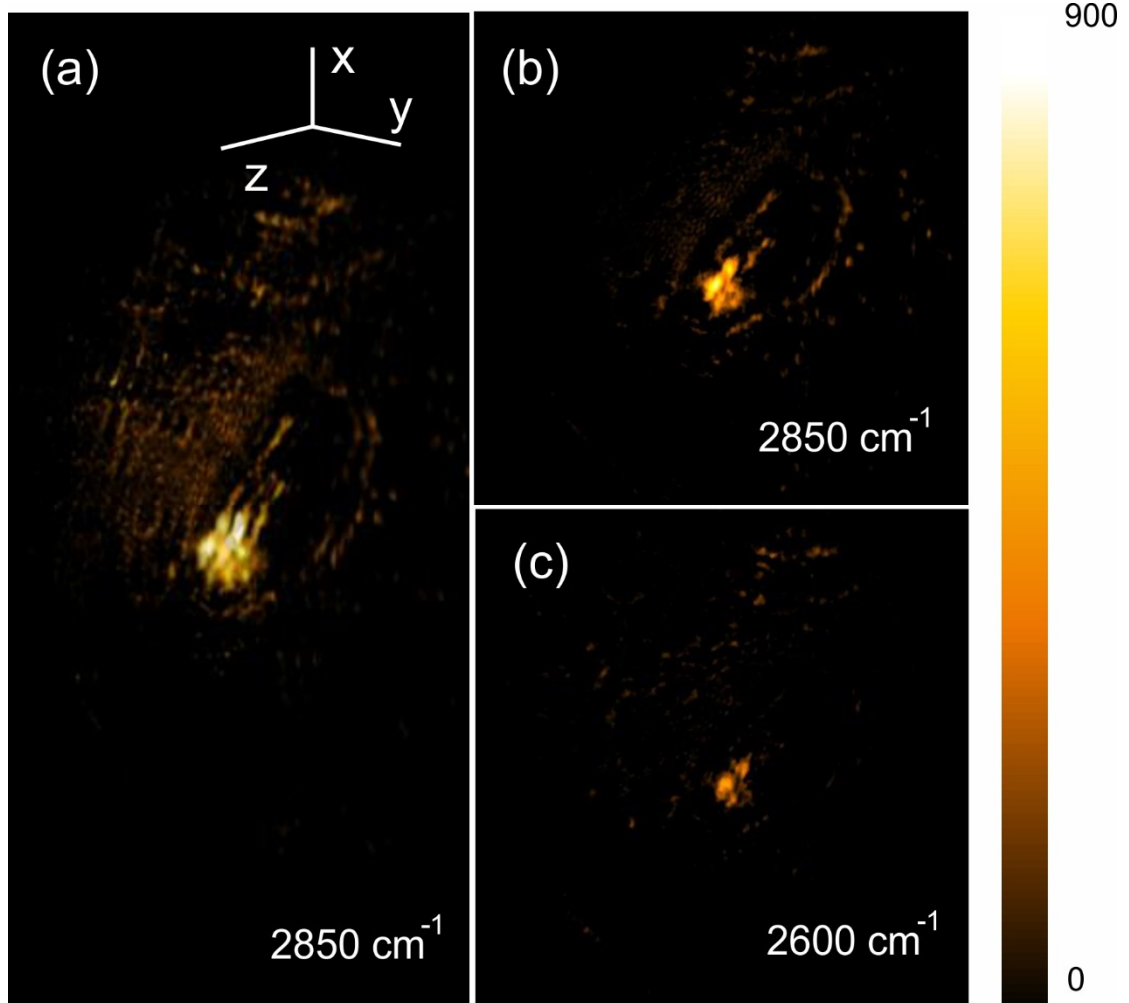


Supplementary Figure S10. Optical imaging of designed resin structure clean (b) and embedded in silicone lubricant (a).



Supplementary Figure S11. Imaging of designed resin structure embedded in silicone lubricant. (a) Full 3D scan (Inset: 3D rendering and optical image), (b) cross section at height (b) $25\text{ }\mu\text{m}$ and (c) $0\text{ }\mu\text{m}$. Total 3D scan 0.5 seconds.

The structures presented in Supplementary Figures SF8 and SF9 were manufactured with the approach outlined in the Methods section of the main text. This particular structure has several fabrication defects and clear differences between the polymerized layers (Supplementary Figure SF9a). If embedded in silicone lubricant, a compound with a strong MIR absorption around 2900 cm^{-1} , it becomes barely visible to the eye due to refractive index matching (Supplementary Figure SF8b). However, the structure is clearly resolved in IR, using our 3D imaging approach (Supplementary Figure SF9) with good contrast if tuned on and off the 2900 cm^{-1} absorption resonance of the silicone lubricant (Supplementary Figure SF10).



Supplementary Figure S13. Imaging of lysozyme crystals on mica glass. (a) 3D reconstructions at 2850 cm⁻¹. 2D image of crystal top at 2850 cm⁻¹ (b) and (c) 2600 cm⁻¹.